Higher Vocational School
and Secondary Technical School of Electrical Engineering
Plzeň, Koterovská 85

YEAR PROJECT

Topic:

Design and Construction of an RC Aircraft Model

Author: Martin Svítek
Class: 3.M
Supervisor: Ing. Pavel Jedlička
Date: 30 April 2026
Grade:

Abstract

This thesis deals with the design and construction of a fixed-wing RC aircraft model. The work covers the entire development cycle of the project including aerodynamic analysis, design of lifting surface geometry, selection of the propulsion system, design of onboard electronics, and implementation of wireless communication between the aircraft and the controller. The aerodynamic analysis was performed using Xfoil and XFLR5 software for Reynolds numbers in the range of 80,000–110,000. The control electronics are based on the ESP32 microcontroller, and wireless communication is implemented using HC-12 modules operating at 433 MHz.

Keywords: RC aircraft, model airplane, aerodynamics, NACA 4412, XFLR5, ESP32, HC-12, wireless communication, 3D printing, fixed-wing

Declaration:

“I declare that I have written this work independently and that I have used only the literary sources and information that I cite and list in the bibliography.”

“I declare that I have used AI tools in accordance with the principles of academic integrity and that I reference the use of these tools in the work in an appropriate manner.”

“I consent to the use of my work by the teachers of VOŠ and SPŠE Plzeň for teaching purposes.”

In Plzeň, date: .... Signature: ....

Contents

Introduction

Building RC aircraft models is a field that brings together several technical disciplines, above all aerodynamics, mechanical design, electronics and programming. Most commercially available models rely on ready-made control units and pre-designed airfoils, so the user never has to understand the principles the aircraft actually works on. This year project takes the opposite approach and covers the whole development cycle of an RC aircraft model, from the basic aerodynamic analysis all the way to the control unit's own software.

The aim of the project is to design and build a working fixed-wing RC aircraft model without using commercial kits or autopilot units. The model is controlled by a custom-built controller with a wireless link and uses 3D-printed parts for the wing and fuselage structure. The project is conceived as a complete case study demonstrating how theoretical principles of aerodynamics and mechanics are applied in practice.

The work is divided into four main chapters. The first chapter covers the aerodynamic background needed for the design: the force balance, lift, drag, airfoils and longitudinal stability. The second chapter applies this knowledge to the actual geometric design of the model, including the choice of the propulsion system and a description of the structure. The third chapter is devoted to the electronics, describing the components used and the wiring diagrams of both parts of the system. The fourth chapter describes the software side of the project, in particular the wireless communication between the controller and the aircraft over HC-12 modules and the firmware implementation on the ESP32 microcontroller.

The aerodynamic analysis was carried out in Xfoil and XFLR5, which are standard tools in both amateur and professional aircraft design.

1 Aerodynamics

This chapter covers the aerodynamic background needed for the design of the aircraft model. It starts from the basic force balance, moves on to the lift equation, and finishes with specific calculations such as the Reynolds number, the tail volume coefficients and the stall speed. All of the equations are then used in Chapter 2 for the geometric design of the model.

1.1 Basic forces

Four main forces act on an aircraft in flight, shown in Figure 1.1: lift L, weight W, thrust T and aerodynamic drag D.

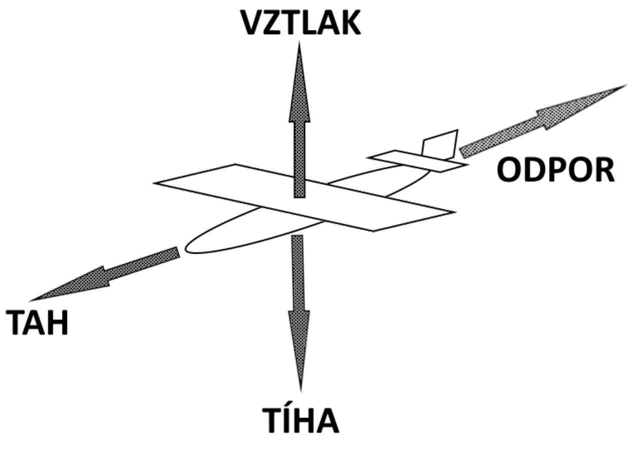

Figure 1.1: The four basic forces acting on an aircraft in flight.

Thrust acts in the direction of flight, air drag acts against the thrust, lift acts perpendicular to the direction of flight, and weight always points towards the ground.

1.2 Force balance in steady flight

In steady, straight, unaccelerated flight the forces are in balance. Lift equals the weight of the aircraft and engine thrust balances the aerodynamic drag

$$L = W \tag{1.1}$$

$$T = D \tag{1.2}$$

where L is lift, W is weight, T is thrust and D is aerodynamic drag.

1.3 Lift

1.3.1 Lift equation

The amount of lift depends on the flight speed, air density, wing area and airfoil shape. Lift is described by the equation

$$L = \frac{1}{2} \rho V^2 S C_L, \tag{1.3}$$

where ρ [$\mathrm{kg\,m^{-3}}$] is the air density, V [$\mathrm{m\,s^{-1}}$] is the flight speed, S [$\mathrm{m^2}$] is the wing area and C_L [–] is the lift coefficient.

From Equation 1.3 and the condition $L = W$, the lift coefficient for steady level flight can be expressed as

$$C_L = \frac{2W}{\rho V^2 S}. \tag{1.4}$$

This is the C_L for steady flight. $C_{L,max}$ is then the maximum lift coefficient; once it is exceeded, the wing stops generating lift and the aircraft stalls. The coefficient $C_{L,max}$ depends on the airfoil shape, the angle of attack and the Reynolds number. The value of $C_{L,max}$ for the main wing was read off the graph from a 2D simulation of the airfoil in XFLR5.

1.3.2 Lift coefficient as a function of angle of attack

C_L grows approximately linearly with the angle of attack α up to a critical value, beyond which the flow separates from the airfoil and lift drops sharply. This relationship is described in detail in Section 1.5.

1.4 Aerodynamic drag

1.4.1 Drag equation

Aerodynamic drag is the force acting against the motion of the aircraft through the air, which the motor has to overcome continuously. Analogously to lift, drag is described by the equation

$$D = \frac{1}{2}\rho V^2 S C_D, \tag{1.5}$$

where ρ [$\mathrm{kg\,m^{-3}}$] is the air density, V [$\mathrm{m\,s^{-1}}$] the flight speed, S [$\mathrm{m^2}$] the wing area and C_D [–] the drag coefficient.

1.4.2 Drag coefficient

The total drag coefficient consists of two main components

$$C_D = C_{D0} + C_{Di}, \tag{1.6}$$

Profile drag C_{D0} is caused by air friction on the wing surface (skin friction) and by pressure losses as the air flows around the airfoil (form drag). It depends on the airfoil shape and the surface quality. Profile drag exists even at zero lift.

Induced drag C_{Di} is a direct consequence of lift. At the wing tips there is a pressure difference between the lower and upper surface, air spills over and forms tip vortices. These vortices tilt the aerodynamic force backwards and increase the total drag. Induced drag grows with increasing lift and decreases with higher wing aspect ratio. Its magnitude can be calculated from the formula

$$C_{Di} = \frac{C_L^2}{\pi \cdot e \cdot AR}, \tag{1.7}$$

where e [–] is the Oswald efficiency factor ($e = 1$ for an ideal elliptical lift distribution, typically $e = 0.85$ for a rectangular wing [1]) and AR [–] is the wing aspect ratio

$$AR = \frac{b^2}{S}. \tag{1.8}$$

1.5 Wing airfoil

1.5.1 Airfoil geometry

The airfoil defines the cross-sectional shape of the wing. Its basic parameters are:

- **Chord** c — the distance between the leading and trailing edge,
- **Camber** — the maximum distance of the mean line from the chord, expressed in % of the chord,

- **Thickness** — the maximum height of the airfoil in % of the chord,
- **Angle of attack** α — the angle between the chord and the velocity vector of the flow.

1.5.2 The NACA series

Airfoils of the NACA series are named systematically by a four-digit code NACA XYZZ, where:

- **X** — maximum camber of the mean line in % of the chord,
- **Y** — position of maximum camber in tenths of the chord from the leading edge,
- **ZZ** — maximum airfoil thickness in % of the chord.

The airfoil designated NACA 0012 is therefore symmetric (zero camber) with a thickness of 12 % of the chord. NACA 4412 has a camber of 4 % of the chord located at 40 % from the leading edge and a thickness of 12 %.

1.5.3 Airfoil choice for this project

The NACA 4412 airfoil was chosen for the main wing. The airfoil has positive camber, thanks to which it generates lift even at zero angle of attack, which is an advantage at the low speeds typical for this model.

The symmetric NACA 0012 airfoil was chosen for the tail surfaces, because these surfaces are supposed to be aerodynamically neutral and generate force only when the control surfaces are deflected from the neutral position.

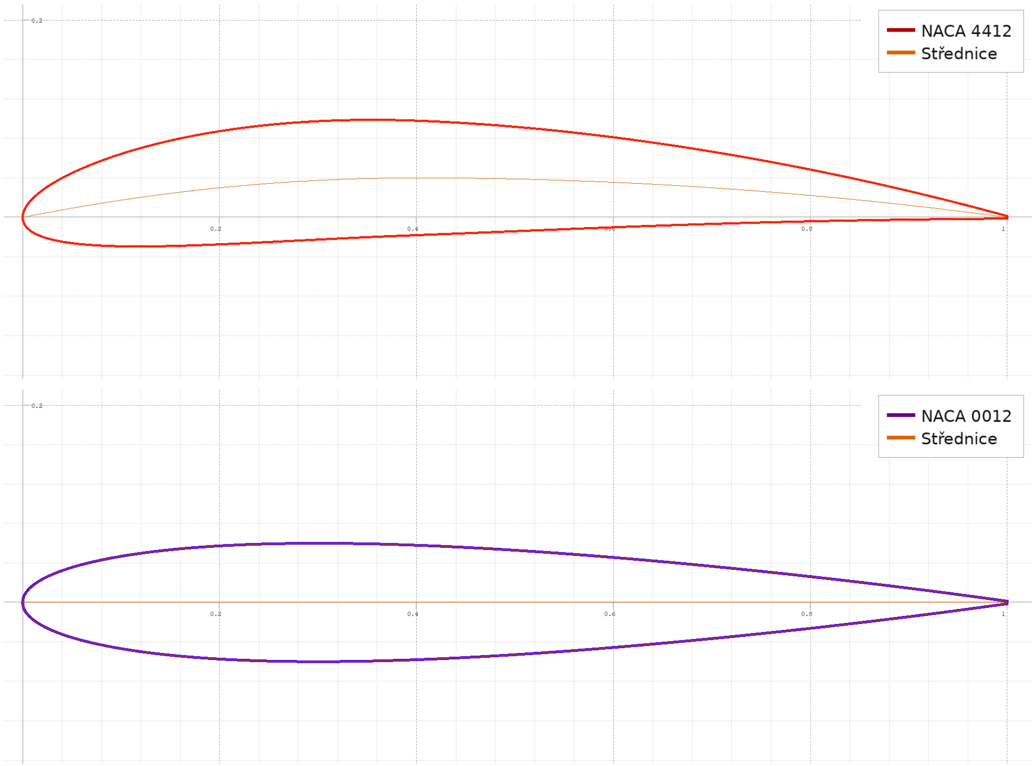

Figure 1.2: NACA 4412 (main wing) and NACA 0012 (tail surfaces) airfoils generated in XFLR5.

1.6 Reynolds number

The Reynolds number is a dimensionless parameter describing the character of the flow in the boundary layer and is defined by the equation

$$Re = \frac{V \cdot c}{\nu}, \tag{1.9}$$

where V [$\mathrm{m\,s^{-1}}$] is the flight speed, c [m] is the chord (the characteristic length) and ν [$\mathrm{m^2\,s^{-1}}$] is the kinematic viscosity of air ($\nu = 1.5 \times 10^{-5}$ $\mathrm{m^2\,s^{-1}}$ under standard conditions).

At $Re < 5 \times 10^5$ the boundary layer remains laminar. RC models typically operate in the range $Re \approx 10^4$–10^5, which brings specific behaviour such as a higher tendency towards laminar boundary layer separation and a worse C_L/C_D ratio compared with full-size aircraft ($Re > 10^6$). This fact limits the accuracy of viscous 3D simulations in programs such as XFLR5, which is why the inviscid VLM1 method was used for the 3D analysis.

For the design speed $V = 12\ \mathrm{m\,s^{-1}}$ and a main wing chord of $c = 0.13$ m we get

$$Re = \frac{12 \cdot 0.13}{1.5 \times 10^{-5}} = 104\,000. \tag{1.10}$$

The model will operate in the range of approximately $Re = 80\,000$–$110\,000$.

1.7 Wing loading

Wing loading is the ratio of the aircraft mass to the main wing area and is defined as

$$WL = \frac{m}{S}, \tag{1.11}$$

where m [kg] is the aircraft mass and S [m^2] the wing area. A lower wing loading means a lower landing speed and better flight characteristics at low speeds.

1.8 Drag polar and glide ratio

The drag polar shows the relationship between C_L and C_D for various angles of attack. The glide ratio K is defined as

$$K = \frac{C_L}{C_D}. \tag{1.12}$$

The higher the glide ratio, the less drag the aircraft generates for a given amount of lift. The aircraft flies most efficiently at the point where the glide ratio K reaches its maximum.

1.9 Horizontal tail volume coefficient

The horizontal tail volume coefficient V_h expresses the stabilising effect of the horizontal stabiliser and is a key parameter for setting the longitudinal stability. It is defined by the equation

$$V_h = \frac{S_h \cdot l_h}{S \cdot c}, \tag{1.13}$$

where S_h [m^2] is the horizontal tail area, l_h [m] is the tail arm, which gives the distance from the aerodynamic centre of the tail to the aerodynamic centre of the main wing, taken at 25 % of the chord of both surfaces, S [m^2] is the main wing area and c [m] is the main wing chord. For a rectangular wing, c equals the chord. For typical light aircraft the recommended range is $V_h = 0.3$–0.6 [7].

1.10 Vertical tail volume coefficient

Similarly to V_h, the coefficient V_v expresses the stabilising effect of the vertical stabiliser (fin) in the directional axis and is defined by the equation

$$V_v = \frac{S_v \cdot l_v}{S \cdot b}, \tag{1.14}$$

where S_v [m^2] is the fin area, l_v [m] is the fin arm, S [m^2] is the main wing area and b [m] is the main wing span. For typical light aircraft the recommended range is $V_v = 0.02$–0.05 [7].

1.11 Stall speed

The stall speed V_{stall} is the minimum flight speed at which the wing still generates sufficient lift. It follows directly from the condition $L = W$ and Equation 1.3 and is given by the formula

$$V_{stall} = \sqrt{\frac{2\,W}{\rho\,S\,C_{L,max}}}, \tag{1.15}$$

where $W = mg$ [N] is the aircraft weight, $\rho = 1.225\ \mathrm{kg\,m^{-3}}$ is the air density (standard ISA conditions) and $C_{L,max}$ [–] is the maximum lift coefficient.

The value of $C_{L,max}$ for a 3D wing cannot be read directly from a 2D airfoil simulation in Xfoil, because the 2D analysis does not account for tip vortices, downwash, or the non-uniform lift distribution along the span. For this reason the 2D value $C_{l,max}$ is converted using the correction coefficient k_{3D} [1].

$$C_{L,max} = C_{l,max} \cdot k_{3D}, \quad k_{3D} = 0.75\text{–}0.85 \tag{1.16}$$

where $C_{l,max}$ [–] is the maximum lift coefficient from the 2D airfoil analysis and k_{3D} [–] is an empirical correction factor accounting for 3D effects.

1.12 Longitudinal stability

An aircraft is statically longitudinally stable if, when the nose is deflected upwards, a moment arises that returns the nose back down, and vice versa. This condition is met when the centre of gravity (CG) lies in front of the neutral point (NP) of the aerodynamic configuration. The static margin (SM) states by how many percent of the chord the centre of gravity lies in front of the neutral point. The larger the SM, the more stable the aircraft. The static margin is given by the formula

$$SM = \frac{x_{NP} - x_{CG}}{\bar{c}} \cdot 100\,\%, \tag{1.17}$$

where x_{CG} is the position of the centre of gravity, x_{NP} is the position of the neutral point and $\bar{c}$ is the mean aerodynamic chord. For RC models the recommended range is

$SM = 5\text{–}15\ \%$ [7].

The aerodynamic moment of the wing is described by the coefficient C_m. The stability condition requires the moment to decrease with increasing angle of attack, i.e.

$$\frac{dC_m}{d\alpha} < 0 \tag{1.18}$$

which means that as the angle of attack α increases, the moment coefficient must fall and the aircraft returns to its equilibrium position on its own.

1.12.1 Control surfaces

The motion of the model about its three axes is controlled by these surfaces:

- **Ailerons** — roll (the x axis). The ailerons work in opposite phase — when one deflects upwards, the other deflects downwards. This creates an asymmetric lift distribution which rolls the model.
- **Elevator** — pitch (the y axis). Deflecting the elevator changes the angle of attack of the tail surface, producing a moment that pitches the nose of the aircraft up or down.
- **Fin** — fixed, with no servo. Directional stability is provided by the geometry of the tail surfaces itself. The exact dimensions of all control surfaces are given in Chapter 2.

2 Model design

This chapter applies the aerodynamic relations from Chapter 1 to the actual geometric design of the model. It describes the dimensions of all lifting surfaces, the calculations of the key parameters and the choice of the propulsion system.

2.1 Requirements and specifications

The model is designed as an RC aircraft with a wingspan of 600 mm and a mass of up to 650 g. The goal is to achieve sufficient lift for stable flight at a speed of 10–12 m/s. The model is equipped with ailerons for roll control and an elevator for pitch control. It is powered by a single brushless motor with a suitable propeller, with a thrust-to-weight ratio sufficient for a fixed-wing model.

2.2 Lifting surface geometry

The designed dimensions of all lifting surfaces are summarised in Table 2.1.

Table 2.1: Overview of the model's lifting surfaces.

Surface	Span	Chord	Airfoil	Area
Main wing	600 mm	130 mm	NACA 4412	0.078 m^2
Horizontal stabiliser	200 mm	80 mm	NACA 0012	0.016 m^2
Vertical stabiliser	80 mm	80 mm	NACA 0012	0.0064 m^2

2.2.1 Main wing

The main wing has a span of 600 mm and a chord of 130 mm, giving an area of $S = 0.078$ m^2. The NACA 4412 airfoil used provides good lift characteristics and at the same time resists flow separation well at the low speeds typical for this model. According to Equation 1.8 the wing aspect ratio comes out to $AR = 4.62$, which is a reasonable value for RC models, balancing induced drag against manoeuvrability. The wing is fitted with ailerons for roll control.

2.2.2 Horizontal stabiliser

The horizontal stabiliser has a span of 200 mm and a chord of 80 mm, giving an area of $S_h = 0.016$ m^2. The NACA 0012 airfoil used is symmetric, which suits a stabiliser that is supposed to be aerodynamically neutral. The elevator flap is deflectable to control the pitch of the aircraft's nose. To calculate the horizontal tail volume coefficient V_h from Equation 1.13, the arm l_h has to be determined; it gives the distance between the aerodynamic centre of the main wing and the aerodynamic centre of the stabiliser. With the designed geometry $l_h = 0.29$ m, which gives $V_h = 0.45$, within the recommended range for light aircraft.

2.2.3 Vertical stabiliser (fin)

The vertical stabiliser (fin) is designed as a trapezoid with a root chord of 100 mm and a tip chord of 60 mm at a span of 80 mm. The mean chord comes out at 80 mm and the area at $S_v = 0.0064\,\mathrm{m}^2$. The NACA 0012 airfoil used is symmetric, which suits a stabiliser that is supposed to be aerodynamically neutral. The fin is fixed, with no deflection, because at this model size and with the designed tail geometry, sufficient directional stability is already provided. To calculate the vertical tail volume coefficient V_v from Equation 1.14, the arm l_v has to be determined; it gives the distance between the aerodynamic centre of the main wing and the aerodynamic centre of the fin. It comes out at $l_v = 0.29$ m, which gives $V_v = 0.041$. The result is within the recommended range for light aircraft.

2.2.4 Control surfaces

The ailerons are located on the outer part of each wing half and are 190 mm long, while the rest of the wing near the fuselage remains fixed. The total aileron length is therefore 380 mm. The flaps are deflected by servomotors to control the roll of the aircraft. The flaps and servos are linked mechanically by pushrods, with the flap deflection set to approximately 20° to provide sufficient controllability without excessive drag. The pushrods are temporarily made from a Merkur construction kit, but in the future they will be replaced with a stiffer and lighter design.

2.3 Centre of gravity and static stability

The centre of gravity (CG) is designed to lie at approximately 28 % of the mean aerodynamic chord (MAC) of the main wing, which provides static stability with a sufficient margin.

The neutral point (NP) was determined by a VLM1 simulation in XFLR5 as $x_{NP} =$ 51.0 mm from the leading edge of the main wing. The centre of gravity is designed at $x_{CG} =$ 41.0 mm from the leading edge, which corresponds to 31.5 % of the mean aerodynamic chord (MAC). The static margin from Equation 1.17 comes out as

$$SM = \frac{51.0 - 41.0}{130} \cdot 100 \approx 7.7\ \%$$

The result lies within the recommended range of 5–15 % for RC models, so the model is statically stable.

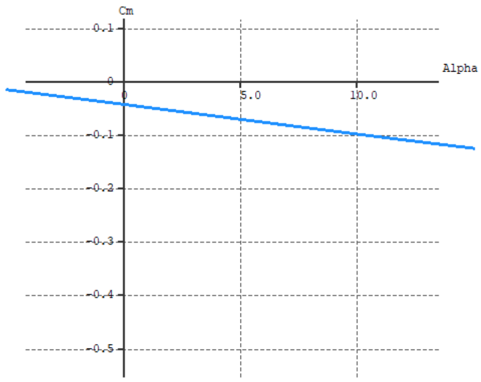

Figure 2.1: Moment coefficient C_m as a function of the angle of attack α from the XFLR5 analysis.

The position of the neutral point was verified by a C_m/α analysis in XFLR5, where the negative slope of the curve in Figure 2.1 demonstrates the stability of the aircraft.

2.3.1 Simulation results

XFLR5 was used to verify the aerodynamic properties of the designed model using the VLM1 method at the design speed $V = 12\,\mathrm{m/s}$ and angles of attack in the range $\alpha = -5°$ to 15°. The angle of 2° was chosen as a representative example corresponding to a typical cruise regime. The model geometry corresponding to the parameters in Table 2.1 is shown in Figure 2.2.

Table 2.2: Results of the VLM1 simulation in XFLR5 at $V = 12\,\mathrm{m/s}$, $\alpha = 2$.

Parameter	Value
Span b	0.600 m
Wing area S	0.078 m
Mass m	0.632 ± 0.005 kg
Lift coefficient C_L	0.407
Drag coefficient C_D	0.012
Glide ratio C_L/C_D	34.78
Moment coefficient C_m	-0.066
Neutral point position x_{NP}	0.051 m
Centre of gravity position x_{CG}	0.041 m

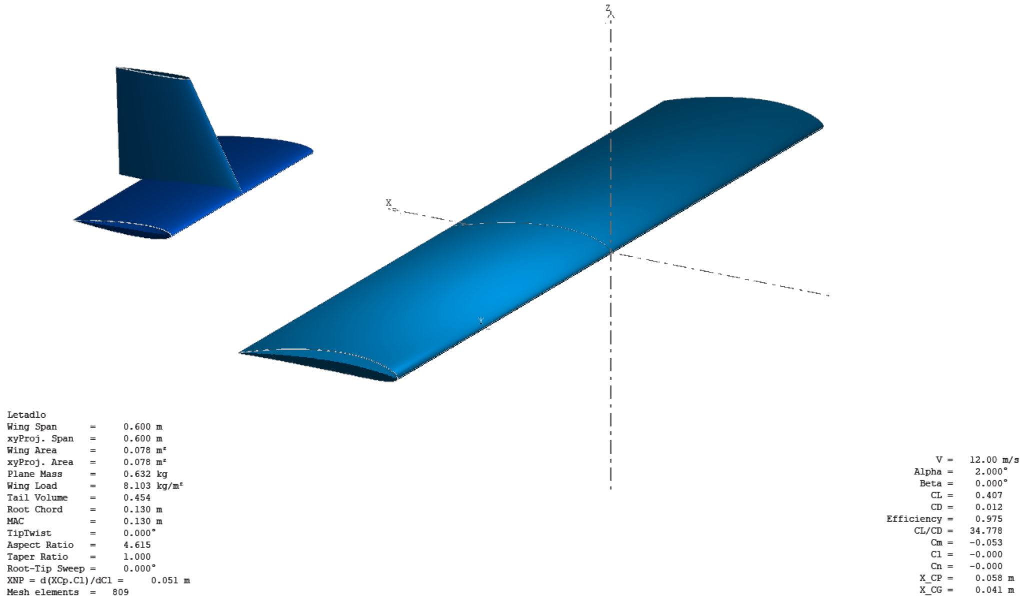

Figure 2.2: 3D model of the aircraft in XFLR5. The simulation parameters are listed in Table 2.2.

Figure 2.3 shows the distribution of aerodynamic force per unit area ($F/s = q \cdot C_p$) over the wing surface. The dominant source of lift is the suction on the upper surface of the wing. The red arrows pointing upwards reach values of up to 58 Pa and represent the suction pulling the wing upwards. The lower surface of the wing contributes to lift by overpressure to a smaller extent. The blue arrows at the leading edge correspond to the stagnation pressure region, where the air impacts the airfoil. The tail surface shows a significantly lower force loading, confirming its stabilising function without a significant contribution to the total drag.

The simulation also confirms the neutral point position $x_{NP} = 0.051\,\mathrm{m}$ and the centre of gravity position $x_{CG} = 0.041\,\mathrm{m}$, from which the static margin calculated in Section 1.12 follows. The glide ratio of the model in this flight regime comes out as $K = 34.8$.

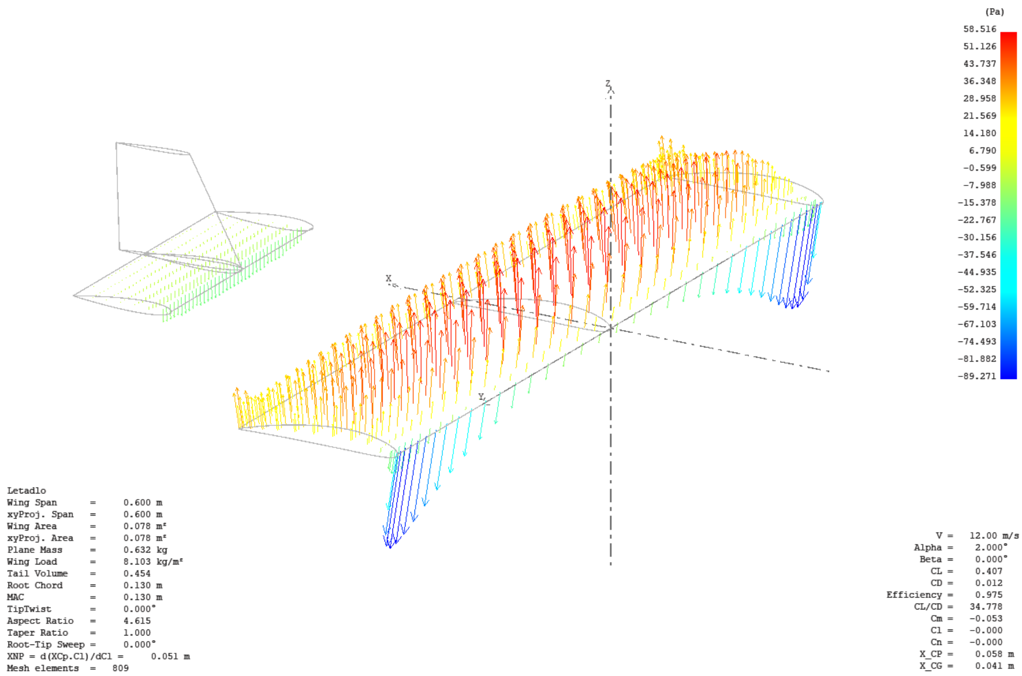

Figure 2.3: Distribution of aerodynamic force per unit area ($F/s = q \cdot C_p$) over the wing surface from the VLM1 analysis at $V = 12\,\mathrm{m/s}$, $\alpha = 2$.

2.4 Stall speed and flight conditions

The maximum lift coefficient $C_{L,max}$ for the 3D wing was determined by correcting the 2D value from Xfoil. From the simulation of the NACA 4412 airfoil at $Re = 104\,000$, the graph in Figure 2.4 gives $C_{l,max} = 1.32$. After applying the correction coefficient $k_{3D} = 0.80$ according to Equation 1.16 we get

$$C_{L,max} = 1.32 \cdot 0.80 = 1.06.$$

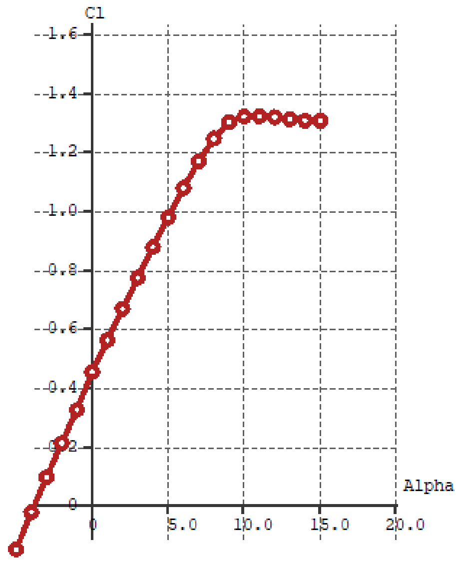

Figure 2.4: Lift coefficient C_L as a function of the angle of attack α from the Xfoil analysis.

The stall speed was calculated from Equation 1.15 for a model mass of $m = 632 \pm 5$ g and comes out as

$$V_{stall} = \sqrt{\frac{2 \cdot 0.632 \cdot 9.81}{1.225 \cdot 0.078 \cdot 1.06}} = 11.1 \pm 0.04\,\mathrm{m/s}.$$

The proposed cruise speed of $V = 12$ m/s is approximately 7.5 % above the stall speed, which is a sufficient safety margin for this model. The wing loading of the model according to Equation 1.11 comes out as

$$WL = \frac{0.632}{0.078} = 8.1 \pm 0.06\,\mathrm{kg/m^2}.$$

The mass values given here are real values obtained by weighing the finished model, including the battery and electronics.

2.5 Propulsion system

2.5.1 Motor and propeller

The KAVAN Brushless C2822-1400KV motor was chosen as the power unit — an outrunner brushless motor intended directly for fixed-wing RC models. It is a low-RPM, high-torque motor, which allows it to drive propellers of larger diameter without a gearbox. The motor has a constant of $KV = 1400$ rpm/V and a mass of 34 g [10].

The propeller recommended by the manufacturer for a 3S supply is an APC 6×4". Because of the higher overall mass of the model, an APC 8×4" propeller was chosen instead; thanks to its larger diameter it moves more air and generates substantially more thrust. This choice raises the current draw above the motor's nominal limit, so full throttle is used only briefly during take-off and climb.

The measured thrust at full throttle ranged between 480–510 g. For further calculations the value $T = 495 \pm 15\,\mathrm{g}$ is used. The thrust-to-weight ratio for the total model mass $m_{MTOW} = 632 \pm 5\,\mathrm{g}$ is

$$\frac{T}{W} = \frac{495}{632} = 0.78 \pm 0.02.$$

For a fixed-wing model this ratio is sufficient. Unlike multicopters, the motor does not have to carry the entire mass, since the wing's lift carries the main part of the weight in flight. The motor serves primarily to maintain a sufficient cruise speed.

2.5.2 ESC and battery

Motor speed is regulated by a Hornet 40 A electronic speed controller (2–4S), which communicates with the control unit via a standard PWM signal. Power is supplied by a KAVAN LiPo 1300 mAh / 11.1 V (3S) / 40–80C battery [11]. The nominal voltage of 11.1 V and the capacity of 1300 mAh are a good compromise between mass and endurance.

2.5.3 Energy budget

The maximum power input of the propulsion system is limited by the KAVAN C2822-1400KV motor to $P_{max} = 90$ W at a current of $I_{max} = 11$ A from a $U = 11.1$ V source (3S LiPo). In cruise flight at roughly 50 % throttle, the motor draw is estimated at $I_{motor} \approx 5.5$ A. The electronics (ESP32, HC-12, 3× MG90S) draw approximately $I_{el} \approx 0.5$ A. The total estimated current draw in cruise is therefore

$$I_{cruise} = 5.5 + 0.5 = 6.0 \text{ A}.$$

The usable battery capacity when discharging to 80 % of the nominal capacity is $1300 \cdot 0.8 = 1040$ mAh. The flight time is calculated as the usable battery capacity divided by the total current draw, converted to minutes. The estimated flight time comes out as

$$t = \frac{1040 \text{ mAh}}{6000 \text{ mA}} \cdot 60 = 10.4 \text{ min}.$$

The KAVAN LiPo 1300 mAh / 40C battery can continuously supply up to 52 A, which covers the maximum motor draw of 11 A with a wide margin. An endurance of 10 minutes is sufficient for test flights.

2.6 Structure and materials

Carbon fibre composite was chosen as the main structural material for the fuselage and wing; it offers an excellent strength-to-weight ratio. The rib profiles of the wing and tail surfaces are 3D printed from PLA. These parts are strong enough for the purpose and allow the airfoil shape to be maintained precisely. The wing surface is covered with heat-shrink film, which provides a smooth aerodynamic surface while adding minimal mass. The main wing and the spine tube are joined by two plates of 4 mm birch plywood, which provide sufficient stiffness and strength to carry the loads during flight. The battery and electronics are located between these plates.

2.6.1 Main wing design

So that the wing keeps the correct and constant airfoil shape along its entire length, it is designed as a sandwich structure made up of ribs, carbon spars and film. The ribs, matching the NACA 4412 airfoil, are 3D printed with lightening holes that also serve as pass-throughs for the servo cables. Two carbon spars (6 mm diameter, 600 mm long) pass through the ribs and provide the torsional and bending stiffness of the wing. There are 16 ribs in total, 8 on each side: 4 in the fixed part and 4 smaller ones in the aileron section. The surface is covered with heat-shrink film, which creates an aerodynamically smooth surface and adds minimal mass. The resulting structure is strong, dimensionally consistent and light.

2.6.2 Fuselage

The main part of the fuselage is a square-section carbon composite tube with 1 mm wall thickness and dimensions of $20 \times 20 \times 355$ mm. This construction provides high stiffness at minimal mass. Wooden plates are attached to both sides of the tube; they serve as the mount for the main wing and as the carrier for the electronics. The horizontal stabiliser slides onto the other end of the tube and is fixed with a screw. The vertical stabiliser (fin) is glued to the horizontal stabiliser and remains fixed, with no servo.

2.6.3 Tail surfaces

The tail surfaces are 3D printed from PLA with a low infill percentage, with the exact NACA 0012 airfoil shape maintained along the entire length. The elevator is driven by a servomotor, while the fin remains fixed with no servo. Directional stability is provided by the geometry of the tail surfaces itself, which simplifies the structure and reduces the overall mass of the model.

2.6.4 Manufacturing process

The model was built in several consecutive steps, working from the central load-bearing structure outwards to the peripheral components.

The basis of the whole model is the square-section carbon spine tube, to which all the other parts connect. Wooden plates of birch plywood were attached to the tube from both sides; they serve as the mount for the main wing and at the same time as the carrier for the electronics placed between them.

Two round carbon rods forming the main wing spars were threaded through the wooden plates. The 3D-printed ribs were then slid onto the rods one by one in the correct order, from the root towards both wing tips. The servomotors driving the ailerons were placed between the inner ribs in the fixed part of the wing.

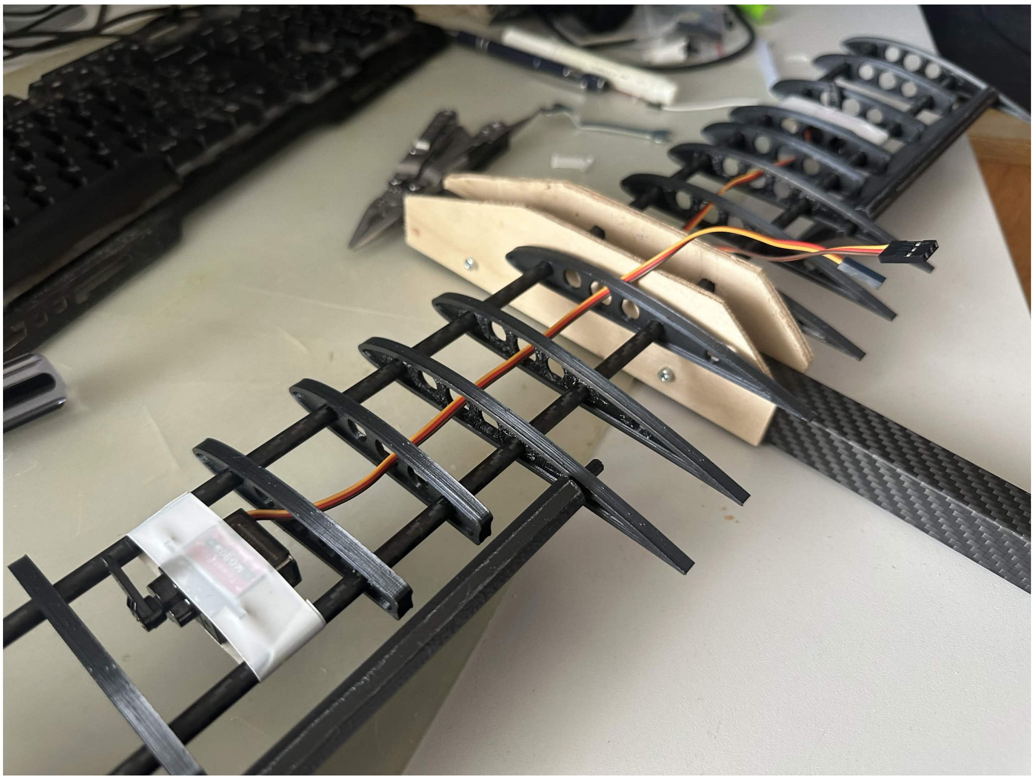

Figure 2.5: The assembled main wing with 3D-printed ribs, carbon spars and integrated cabling.

At the front of the model, a square wooden motor mount with five holes is glued to the fuselage: four for the screws fixing the motor and one central hole for the shaft to pass through. This mount is firmly bonded to the fuselage with epoxy adhesive and is able to transfer the motor thrust into the load-bearing structure.

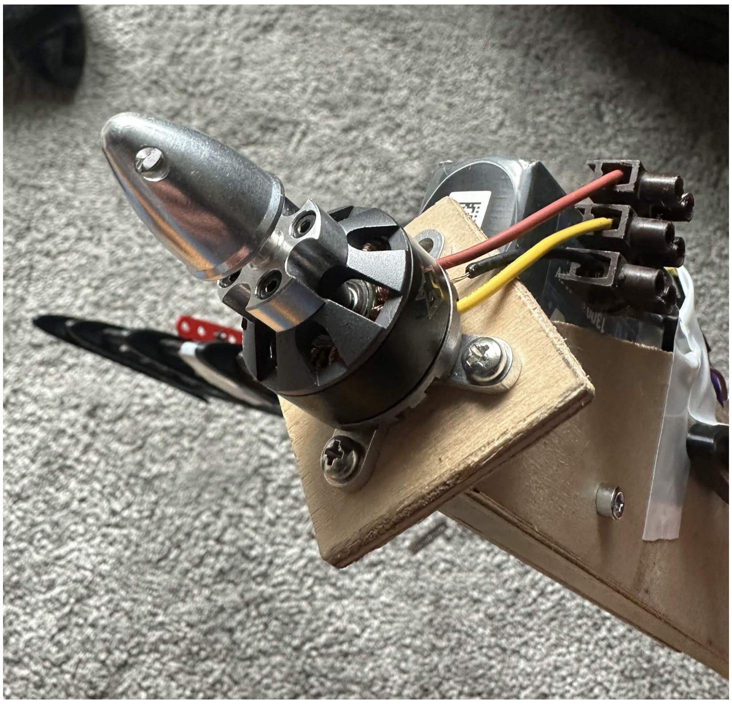

Figure 2.6: Detail of the motor section with the installed KAVAN C2822-1400KV motor and the spinner.

At the rear of the model, the 3D-printed tail surfaces are slid into the fuselage. The horizontal stabiliser is fixed to the fuselage with a screw and the vertical stabiliser is glued to the horizontal one. The elevator servo is mounted on the fuselage in front of the tail surfaces and is connected by a mechanical pushrod.

The final step was installing the electronics between the wooden fuselage plates: mounting the ESP32, the HC-12 module and the ESC, connecting the servomotors to the control unit and placing the battery as close to the nose of the model as possible in order to achieve the correct centre of gravity position.

3 Electronics

The electronics of the model consist of two separate units — the aircraft and the controller — linked by a wireless connection over HC-12 modules. This chapter describes all the components used, the wiring diagram and the power architecture of both units. A detailed description of the software side is given in Chapter 4.

3.1 Wiring diagrams

3.1.1 Aircraft diagram

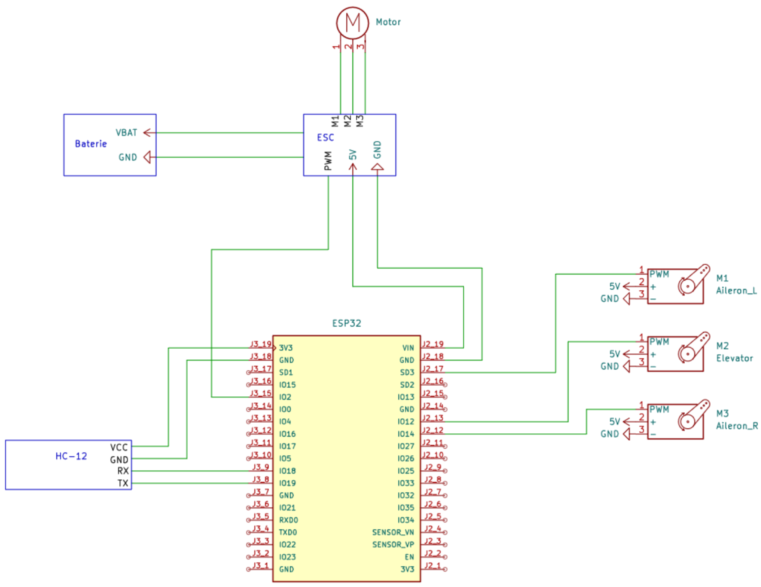

Figure 3.1: Wiring diagram of the aircraft electronics

3.1.2 Controller diagram

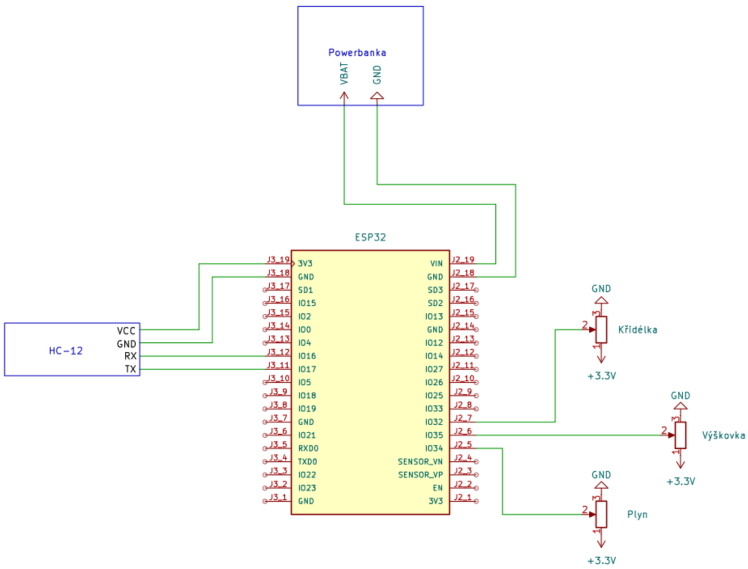

Figure 3.2: Wiring diagram of the controller electronics

3.2 Component overview

Tables 3.1 and 3.2 summarise all the key components of both units.

Table 3.1: Components — aircraft.

Component	Description
ESP32	Main control unit
HC-12	Wireless receiver
MG90S × 3	Servomotors (wings, elevator)
Hornet 40 A ESC	Electronic speed controller
KAVAN C2822-1400KV	Brushless motor
LiPo 3S 1300 mAh	Main battery
APC 8×4"	Propeller
Other	Cables, connectors, mounts

Table 3.2: Components — controller.

Component	Description
ESP32	Controller control unit
HC-12	Wireless transmitter
Joystick 1	Roll/pitch control
Joystick 2	Throttle control
Power bank	Controller power supply

3.3 Component descriptions

3.3.1 ESP32 microcontroller

The ESP32 is a 32-bit microcontroller made by Espressif Systems with a dual-core Xtensa LX6 processor clocked at 240 MHz [6]. What matters for this project is the availability of several hardware UART interfaces, a 12-bit ADC for reading analog inputs, and a sufficient number of PWM outputs for driving the servos and the ESC. The microcontroller is used both in the aircraft (receiver) and in the controller (transmitter), which simplifies firmware development. Both devices share the same platform and the Arduino IDE development environment.

3.3.2 HC-12 wireless module

The HC-12 is a ready-made wireless transceiver operating in the 433 MHz band, described in detail in Section 4.2. From the hardware point of view it is a 5-pin module communicating over a UART interface with a 3.3 V supply voltage. The module contains an integrated antenna, which can be replaced with an external one to increase the range if needed. For this project, however, the integrated antenna is entirely sufficient.

3.3.3 MG90S servomotors

The MG90S is a miniature servomotor with metal gears weighing 13.4 g. Compared with plastic gears, metal gears offer better resistance to landing impacts and a longer service life under repeated loading. The basic parameters are summarised in Table 3.3.

Table 3.3: Parameters of the MG90S servomotor [9].

Parameter	Value
Supply voltage	4.8–6.0 V
Torque	1.8 kg·cm (at 4.8 V)
Speed	0.1 s / 60° (at 4.8 V)
Mass	13.4 g
Interface	PWM 50 Hz, pulse 1000–2000 µs

A total of three MG90S units are used in the model: two for the ailerons and one for the elevator.

3.3.4 Joysticks

The controller is fitted with two dual-axis joysticks that work on the potentiometer principle. One joystick controls roll and pitch and the other controls the throttle. The joystick outputs are read as analog values through the ADC pins of the ESP32, then mapped onto the corresponding PWM signal range and sent over the HC-12 to the aircraft.

3.3.5 ESC and motor

The Hornet 40 A electronic speed controller (2–4S LiPo) drives the brushless motor with a three-phase PWM signal. The input signal from the ESP32 is standard servo PWM (50 Hz, 1000–2000 µs), where 1000 µs corresponds to zero RPM and 2000 µs to full throttle. The ESC contains an integrated BEC (*Battery Eliminator Circuit*), which serves as the 5 V source for the ESP32 and the rest of the electronics.

The KAVAN Brushless C2822-1400KV is a brushless motor whose KV value gives the number of revolutions per minute per volt of supply voltage. When powered from a 3S LiPo (11.1 V), the theoretical no-load speed is therefore approximately $1400 \times 11.1 = 15\,500$ rpm. The measured thrust with the APC 8×4" propeller on 3S reaches approximately 490 g.

3.3.6 Power supply — LiPo battery

The main energy source is a KAVAN LiPo 1300 mAh / 11.1 V (3S) / 40–80C battery. The three-cell configuration (3S) provides a nominal voltage of 11.1 V and 12.6 V when fully charged. The 40C discharge rating means the battery can continuously deliver a current of up to 52 A, which covers the needs of the motor and the electronics with a wide margin. The battery is connected to the ESC with an XT60 connector, which provides a safe and reliable connection.

3.4 Controller — hardware implementation

An old RC drone controller was used as the controller. Only the original joysticks were kept and everything else was removed. An ESP32 was placed inside the controller body and there is an opening in the front of the controller for the HC-12. The controller is powered by a power bank, which provides a stable voltage for the ESP32 and the HC-12.

4 Software and communication

This chapter describes the software architecture of the remote control system. Communication between the controller and the aircraft runs over HC-12 modules operating at 433 MHz. The chapter also covers the structure and key parts of the firmware of both devices.

4.1 System architecture

The system consists of two independent devices. The controller reads the values from the joysticks, packs them into a data structure and sends them wirelessly over the HC-12. The receiver in the aircraft waits for incoming packets, decodes them and sets the corresponding servo positions and motor speed. Both devices use an ESP32 microcontroller and identical HC-12 modules.

4.2 HC-12 communication module

4.2.1 Operating principle and parameters

The HC-12 is a ready-made wireless module operating in the 433 MHz band with an integrated Si4463 radio chip. From the microcontroller's point of view it behaves like a standard serial line (UART). Everything that arrives at the TX pin of one module appears on the RX pin of the other module. There is therefore no need to deal with any RF parameters or install special libraries. The line-of-sight range of the module is several hundred metres, which is entirely sufficient for the purposes of this project.

The key parameters of the module are summarised in Table 4.1.

Table 4.1: Parameters of the HC-12 module [5].

Parameter	Value
Frequency band	433.4–473.0 MHz
Supply voltage	3.2–5.5 V
Default baud rate	9600 Bd
Transmitter power	up to 20 dBm (100 mW)
Interface	UART

4.2.2 Module configuration

The HC-12 is configured with AT commands while the SET pin is held at logic zero. In normal operation SET is at logic one and the module relays data transparently. This project uses the default settings (9600 Bd, channel 1), which require no configuration change.

The wiring of the HC-12 to the ESP32 is identical on both devices:

- **VCC** → 3.3 V
- **GND** → GND
- **TXD** (HC-12) → RX (ESP32)
- **RXD** (HC-12) → TX (ESP32)
- **SET** → HIGH (normal operation)
- **ANT** → antenna

4.2.3 Antenna

This project uses the integrated antenna of the HC-12 module, which provides sufficient range for communication between the controller and the aircraft. If a longer range is ever needed, the integrated antenna can be replaced with an external one, for example a quarter-wave whip antenna connected to the ANT pin.

4.2.4 Data format

The control values are transmitted as a binary data structure (*struct*). Binary transmission is more efficient than a text format: exactly 6 bytes are transmitted instead of dozens of ASCII characters, which reduces latency.

Listing 4.1: Data structure of the control packet.

```
struct Data {
    int16_t throttle;   // throttle:  0 to 4095
    int16_t pitch;      // elevator:  0 to 4095
    int16_t roll;       // ailerons:  0 to 4095
};
```

Using the type `int16_t`, a 16-bit signed integer, guarantees step precision and a constant size of 2 bytes per channel regardless of the platform.

4.3 Transmitter code (controller)

4.3.1 Code structure

The controller software performs three operations in its main loop: it reads the current values from the analog inputs, stores them in the `Data` structure and sends the structure as a block of bytes over the HC-12. The loop repeats approximately every 50 ms, giving a transmit rate of 20 Hz.

4.3.2 Reading the inputs

Joystick 1 provides two analog outputs, the X and Y axes. Joystick 2 serves as the throttle control. The values are read through the 12-bit ADC of the ESP32 and mapped onto the range matching the data structure.

4.3.3 Sending the data

Listing 4.2: Sending a packet from the controller.

```
void loop() {
    packet.throttle = analogRead(THROTTLE_PIN);
    packet.pitch    = analogRead(PITCH_PIN);
    packet.roll     = analogRead(ROLL_PIN);

    HC12.write((uint8_t*)&packet, sizeof(packet));
    delay(50); // 20 Hz
}
```

4.4 Receiver code (aircraft)

4.4.1 Receiving and decoding the data

The receiver waits until a complete packet (6 bytes) is available in the buffer. Once the data arrives, it reads it into the `Data` structure and passes it on to drive the servos and the ESC. The values are then mapped from the range 0–4095 (12-bit ADC) onto the range 1000–2000 µs for the PWM signal.

Listing 4.3: Reception and control on the aircraft side.

```
void loop() {
    if (HC12.available() >= sizeof(packet)) {
        HC12.readBytes((uint8_t*)&packet, sizeof(packet));

        esc.writeMicroseconds(map(packet.throttle, 0, 4095, 1000, 2000));
        servoElevator.writeMicroseconds(map(packet.pitch, 0, 4095, 1000, 2000));
        servoAileronL.writeMicroseconds(map(packet.roll,  0, 4095, 1000, 2000));
        servoAileronR.writeMicroseconds(map(packet.roll,  0, 4095, 2000, 1000));

        lastPacketTime = millis();
    }
}
```

4.4.2 Driving the servomotors and the ESC

Both the servomotors and the ESC are driven by a PWM signal with a period of 20 ms (frequency 50 Hz). A pulse width in the range 1000–2000 µs corresponds to the full range of servo travel or motor throttle. The values from the received packet are mapped onto this range and passed to the appropriate output pins of the ESP32.

4.4.3 Fail-safe

A fail-safe mode is implemented in the aircraft: if no packet arrives for longer than a set time, the aircraft automatically sets the throttle to zero and centres all the servos. This prevents uncontrolled flight in the event of a link failure.

Conclusion

The aim of this year project was the design and construction of a fixed-wing RC aircraft model. The lifting surfaces of the model were designed on the basis of an aerodynamic analysis, a propulsion system was chosen and the electronics were designed, including the remote control system.

The aerodynamic analysis in Xfoil and XFLR5 confirmed that the chosen NACA 4412 airfoil is suitable for the given range of Reynolds numbers and verified the static longitudinal stability of the designed configuration. The static margin came out as $SM = 7.7\,\%$, which is within the recommended range for RC models.

The wireless communication between the controller and the aircraft was successfully tested; the HC-12 modules reliably transmit the control data at 433 MHz with a transmit rate of 20 Hz. The implemented fail-safe mode ensures that in the event of a link failure the aircraft automatically sets the throttle to zero and centres all the servos.

During the construction of the model it turned out that the mass of the 3D-printed tail surfaces has a significant effect on the position of the centre of gravity. The original version of the tail weighed 92 g, which shifted the centre of gravity several tens of millimetres backwards, outside the recommended range. The problem was solved by reprinting the tail surfaces with a lower infill density and thinner walls, which reduced the tail mass to 50 g. This experience confirms that for 3D-printed models, mass estimates have to be part of the design process from the very beginning.

The flight tests will be completed after the final covering of the wing with heat-shrink film. In future iterations the work can continue by adding more features, such as a GPS module, or by moving to a more powerful control unit capable of autonomous stabilisation using a gyroscope and accelerometer.

Bibliography

[1] ANDERSON, John D. *Introduction to Flight*. 8th ed. New York: McGraw-Hill Education, 2017. ISBN 978-1-259-25408-5.

[2] NASA Glenn Research Center. *The Drag Equation* [online]. 2022 [cited 2026-04-10]. Available at: https://www.grc.nasa.gov/www/k-12/VirtualAero/BottleRocket/airplane/drageq.html

[3] DRELA, Mark and Harold YOUNGREN. *XFOIL: Subsonic Airfoil Development System* [online]. 2013 [cited 2026-04-10]. Available at: https://web.mit.edu/drela/Public/web/xfoil/

[4] *XFLR5: Analysis tool for airfoils, wings and planes* [online]. 2022 [cited 2026-04-10]. Available at: http://www.xflr5.tech/xflr5.htm

[5] *HC-12 Wireless Serial Port Communication Module — Datasheet* [online]. [cited 2026-04-10]. Available at: https://www.hc01.com/downloads/HC-12%20english%20datasheets.pdf

[6] Espressif Systems. *ESP32 Series Datasheet* [online]. 2023 [cited 2026-04-10]. Available at: https://www.espressif.com/sites/default/files/documentation/esp32_datasheet_en.pdf

[7] DRELA, Mark. *Lab 8 Notes – Basic Aircraft Design Rules* [online]. Massachusetts Institute of Technology, Unified Engineering, 2006 [cited 2026-04-25]. Available at: https://ocw.mit.edu/courses/16-01-unified-engineering-i-ii-iii-iv-fall-2005-spring-2006/ffbff8a4985ee6ea819afb90c40834e3_spl8.pdf

[8] NASA GLENN RESEARCH CENTER. *The Lift Equation* [online]. 2022 [cited 2026-04-25]. Available at: https://www1.grc.nasa.gov/beginners-guide-to-aeronautics/lift-equation/

[9] TOWER PRO. *MG90S Micro Servo — Datasheet* [online]. [cited 2026-04-26]. Available at: https://www.electronicoscaldas.com/datasheet/MG90S_Tower-Pro.pdf

[10] KAVAN EUROPE. *KAVAN Brushless motor C2822-1400* [online]. [cited 2026-04-26]. Available at: https://kavanrc.com/en/item/product-140793

[11] KAVAN EUROPE. *KAVAN Li-Po 1300 mAh/11.1 V 40/80C 14.4 Wh* [online]. [cited 2026-04-26]. Available at: https://www.kavanrc.com/en/item/kavan-li-po-1300mah-11-1v-40-80c-14-4wh-140749

List of Figures

Appendices

Appendix I — Source code

Appendix II — Wiring diagrams

Appendix III — Photo documentation